JTTEE5 12:416-426

Determination of Cracking Resistance of Thermal Spray Coatings During Four-Point Bend Testing Using an Acoustic Emission Technique

J. Voyer and H. Kreye

(Submitted 25 January 2002; in revised form 22 March 2002)

An acoustic emission (AE) technique was used for the determination of the onset of cracking of thermal spray self-fluxing NiCrFeBSi coatings under tensile loading using a 4-point bend testing apparatus. These coatings were flame sprayed on 42CrMoS4 cylinders having different diameters. Two different post-treatment fusing processes, induction, and flame fusing, were used. Along with the investigations of the effect of cylinder diameters and fusing processes onto the cracking resistance of the coatings, the effect of the same two parameters on the residual stresses was also investigated. Results show that, independently of the diameter of the cylinder, the flame-fused coatings possess a higher cracking resistance than their induction-fused counterparts, i.e., that the strain to fracture is higher for the flame-fused coatings. A correlation between the strain to fracture and the residual strain in the coatings has been established. This study points out that the combination of an AE technique with a bending test apparatus shows some major benefits to obtain important information on the relative ductility of thermal spray coatings.

Keywords acoustic emission technique, bend testing, cracking resistance, self-fluxing NiCrFeBSi, thermal spray coatings

1. Introduction

Thermal spray coatings are widely used in numerous industrial applications for overcoming, for instance, wear and corrosion issues. The development of these thermal spray coatings introduces the need for the characterization and the comparison of the properties of different type of coatings. Besides the determination of the wear and corrosion behavior of these coatings, their characterization also usually involves the measurement of mechanical properties such as hardness measurement and adhesion evaluations. For each of these properties, well-known standardized and easily performed test methods exist.

However, one important mechanical property is the cracking resistance or fracture toughness. This property is especially important for wear behavior of coatings since wear usually involves crack initiation and propagation processes. However, it is also very important for other specific applications. As an example, thermal spraying processes or post-treatment techniques may induce some bending of the samples. To straighten these samples for their respective applications, they have to be bent in the opposite direction with an amount of strain that has to exceed the elastic limit of the base material. Therefore, the measurement of the fracture toughness of the coating gives a limit for the strain to fracture that a coating can experience during the straightening process. However, the fracture toughness is often measured for bulk materials only, but due to the different microstructures and the presence of defects in coatings, these bulk values do not necessarily correspond to those of thermal spray coatings. Therefore, there is a need for the implementation of an easy, fast and reliable test method for the determination of the crack resistance of thermal spray coatings.

Bending tests are fast and easily implemented test methods with which some mechanical properties of the coatings, such as the modulus of elasticity and the yield strength, can be determined. These bending tests have also proven to be efficient for obtaining important knowledge of the cracking resistance of coatings, but only with the combination of a method, such as microscopy, which enables the determination of the onset of cracking.[1-6] However, the use of microscopy for determining the onset of cracking during bending tests has several disadvantages. The major drawback is that the bending load has to be applied by small increments to the sample, and at each load increment, the sample has to be checked by microscopy to determine the presence or the absence of cracks in the coating. Even if the bending apparatus and the sample are small enough to be inserted in a SEM chamber, which is rarely the case, this procedure is quite time-consuming and could give rise to important errors in the evaluation of the cracking resistance of the coatings if the load increments are not small enough to determine precisely the onset of cracking.

Acoustic emission technique has proved to be an excellent method for the detection of irreversible degradation mechanisms occurring inside a material, which is under stress.[1-3,7-10] Different processes, such as crack initiation and propagation, are responsible for the production of ultrasonic waves, also called acoustic emission signals, in materials, which are under mechanical, thermal or chemical stress. Once these ultrasonic waves have been produced, they propagate throughout the stressed sample, giving rise to vibrations of the material surfaces. By using adapted acoustic receivers, these AE signals can

J. Voyer and **H. Kreye,** University of the Federal Armed Forces, Holstenhofweg 85, 22043 Hamburg, Germany. Contact e-mail: joel.voyer@unibw-hamburg.de.

be recorded and analyzed for the determination of the cracking resistance of the coatings. The major advantage of this technique is that it enables the possibility of inspecting the whole sample in real time and in only one test without any load increments.

This work proposes a 4-point bending test combined with an acoustic emission detection technique as a tool for cracking resistance investigations of self-fluxing NiCrFeBSi coatings on steel substrates.

2. Experimental Procedure

2.1 Materials, Coatings, and Post-Treatment Processes

Self-fluxing NiCrFeBSi coatings were produced by powder flame spray technique on 42CrMoS4 cylinders (low alloy ferritic heat treated steel with 1.05% Cr, 0.75% Mn, 0.42% C, 0.40% Si, 0.23% Mo, 0.04% P, and 0.03% S). The nominal composition of the coating is presented in Table 1. Three different diameters were used for the cylinders: 50, 70, and 100 mm but all cylinders had the same length of 800 mm. For each diameter, 2 cylinders were sprayed for a total of 6 cylinders. Following the spraying process, a set of three cylinders, each having a different diameter, was fused using a flame process and the other set of three cylinders were fused using an inductive process. Table 2 gives an overview of the different samples produced for this study.

Both fusing processes, inductive and flame consisted of pre-heating the cylinders to a temperature of 400 °C to avoid or reduce the distortion of the samples. Following this pre-heating step, the densification of the sprayed coatings was performed and this resulted in a significant reduction of the porosity of the coatings. Besides improving the density of the coatings, the fusing process also increases the bonding to the substrate by creating a metallic bond, produces a higher hardness and enhances the surface finish of the coatings. The major differences between the two fusing processes is that both the fusing and cooling time using the inductive process is relatively shorter than with the flame process.

Following the fusing process, the surface of the six cylinders were machined and polished using standard procedures to obtain a near mirror finished surface. For all cylinders, the average thickness of the coatings after machining and polishing was approximately 400 μm, as shown in Table 2.

For each cylinder, a section of the rod having a length of 150 mm was cut from the initial cylinders. Following that, 4 rectangular samples (10 × 10 × 150 mm) were cut from the cylinders using a spark erosion technique. Each sample was cut along the length of the cylinders and at 90° angle from each other. A typical cutting layout of the cylinders is shown in Fig. 1.

2.2 Bend Testing

The bend testing was performed using a tensile machine (Model UPM-60, Schenck-Trebel GmbH, Ratingen, Germany) on which an adapted 4-point bend testing apparatus was mounted. A schematic of the apparatus used for the bend testing is shown in Fig. 2. The tensile machine was used in the compression mode with the lower jaw being stationary and therefore, the load was applied on the inner span of the 4-point bend test apparatus. The samples were inserted in such a way that the bend test apparatus caused the coatings to experience a tensile stress state. The applied crosshead speed of the tensile machine was 14.4 mm/min for all samples. During the bend test, the force applied was measured using a load cell installed on the tensile machine and the deflection of the samples was measured directly at mid-span using a displacement gauge and both of them were connected to a monitoring computer.

The procedure of the bending tests consisted of applying an increasing force on the samples. Once the first occurrence of AE signals was detected by the monitoring system, the force was noted and the tests were continued until reaching a load being approximately 2000 N higher than the previously noted load

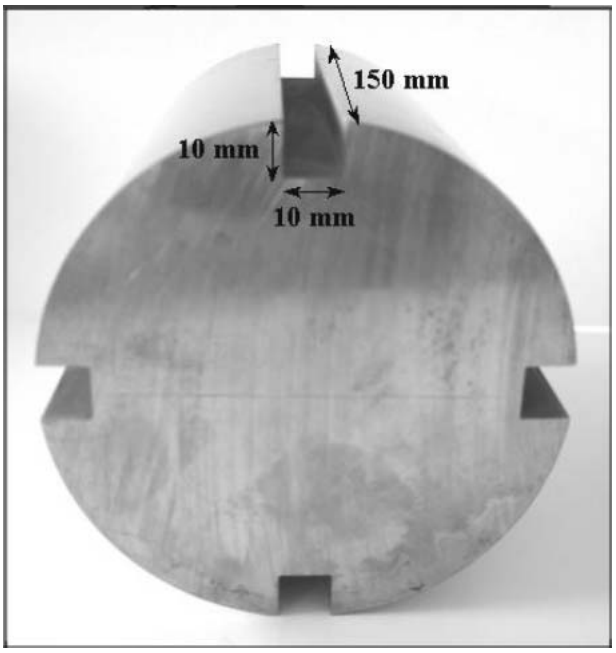

Fig. 1 Typical cutting layout of the rectangular samples from the thermal sprayed cylinders

Table 1 Nominal Composition of the Coating

Element	Minimum wt.%	Maximum wt.%
Ni	Balance	Balance
Cr	7.5	10
Si	3	4
Fe	3	4
B	1.5	2.25
C	0.05	0.5

Table 2 Diameter of the Sprayed Cylinders, Coatings Thickness, and Fusing Process Parameters

Sample Number	Rod Diameter, mm	Coating Thickness, μm	Fusing Process
1	50	400	Induction
2	70	480	Induction
3	100	330	Induction
4	50	385	Flame
5	70	400	Flame
6	100	385	Flame

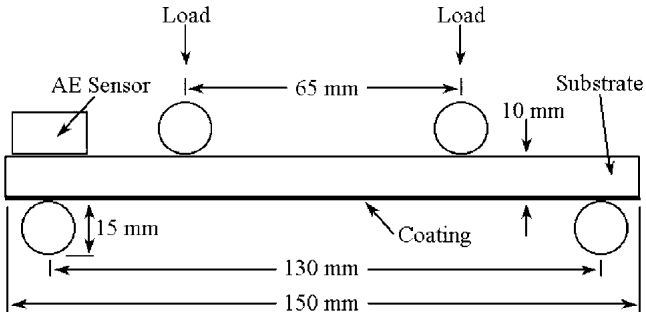

Fig. 2 Schematic illustration of the 4-point bend testing apparatus

Table 3 Parameters of the AE Acquisition System

Parameter	Value
Threshold (dB)	58
Programmable gain (dB)	34
Sampling frequency (MHz)	5
Time resolution (μs)	0.2
Number of points	2048
Pre-trigger (μs)	40

value. For all the coatings, this final load value was in the range of 9000 and 12 000 N. The force value necessary for the first detection of an AE signal was noted only to ensure that the final load value was much higher than the force needed for the onset of cracking of the coatings. However, a more precise analysis was performed after the tests to identify precisely the load value required for the cracking of the coatings. The force and the deflection measured during the tests were transformed, after the completion of the tests, to stress and strain values using the following equations valid only for 4-point bend tests[3,11]:

$$|\text{Stress (MPa)}| = \frac{1.5F(L_2 - L_1)}{bh^2} \quad \text{(Eq 1)}$$

$$|\text{Strain (\%)}| = \frac{436Dh}{L_2^2} \quad \text{(Eq 2)}$$

where F is the force applied in N, L_2, and L_1 are the outer and inner span of the 4-point bend test apparatus in millimeters (L_2 = 130 mm and L_1 = 65 mm as seen in Fig. 2), b is the sample's width (~10 mm), h is the thickness of the sample (~10 mm), and D is the deflection of the sample at mid-span in millimeters. It is worth noting that Eq 1 and 2 give the stress and strain values at the outer surfaces of the samples independently of the fact that the surface is either in compression or in tension, and this is shown by the presence of the absolute value signs in Eq 1 and 2. Therefore, the outer surface of the coatings, which were inserted in the bend testing apparatus as to experience a tensile stress state, has a positive stress or strain value (tensile stress and strain) whereas the backside of the substrate has a negative stress or strain value (compressive stress and strain). However, the stress and strain values inside the coating and in the substrate are lower than these calculated values. The width and thickness of each tested sample were precisely measured using a caliper prior to perform each bending test. For each fusing process and cylinder diameter, only 3 samples out of 4 were tested for a total of 18 bend test measurements and the 4th sample were kept for future measurements.

The modulus of elasticity of a sample can be calculated from the curve force-displacement obtained during a typical bend test [11]:

$$\text{Modulus of Elasticity} = \frac{11L_2^3}{64bh^3} \times \Delta \quad \text{(Eq 3)}$$

where Δ is the slope of the linear section of a typical curve force-displacement and the other variables have been explained in the previous two equations.

2.3 Acoustic Emission Acquisition System

During the bend testing, continuous acoustic emission monitoring was performed to acquire signals caused by the formation and propagation of cracks in the coatings and therefore, to evaluate the stress required to initiate cracking in the coatings. The system used for the acquisition of the acoustic emission signals consisted of a piezoelectric sensor (Model VS150-M, Vallen-Systeme GmbH, Icking, Germany), a pre-amplifier (Model AEP3, Vallen-Systeme GmbH) coupled to a Windows 95-based computer running an AE acquisition and analysis software (Vallen VisualAE software, Vallen-Systeme GmbH).

The sensor was placed at one end of the samples, as shown in Fig. 2, and on the opposite side of the coating to eliminate any modification of the acoustic emission propagation properties due to the presence of cracks in the coatings. The sensor and pre-amplifier have an acoustic response range between 100 and 450 kHz and 95 and 1000 kHz, respectively. To enhance the transmission of acoustic emission signals from the samples to the sensor, silicone-based grease was used at the interface between the sensor and the samples and the sensor was pressed against the samples backside using a rubber tape.

The parameters used for the acquisition of the acoustic signals are presented in Table 3. The threshold was set high enough to eliminate any signals coming either from the movement of the bending machine, from the laboratory environment or from any mechanisms causing AE originating from the substrate material. The determination of this threshold was performed by using uncoated substrates and adjusting the threshold at a value where no signals were detected.

Besides performing the acquisition, Vallen VisualAE software was also used for the analysis and visualization of the acquired acoustic emission signals. This analysis consisted of extracting relevant parameters from each signal acquired and plotting these parameters in graphs relative to the applied force. Three parameters, which give important information on the degree of cracking, were selected and these parameters are: the cumulative number, the cumulative amplitude and the cumulative energy of the AE signals acquired during a complete bending test.

For each sample, an onset of cracking was determined by three different procedures using the three selected parameters: the first occurrence of an AE signal, the first major AE amplitude increase, and the first major AE energy increase.

Once the three values of the onset of cracking were identified using the three procedures, the force applied and the deflection

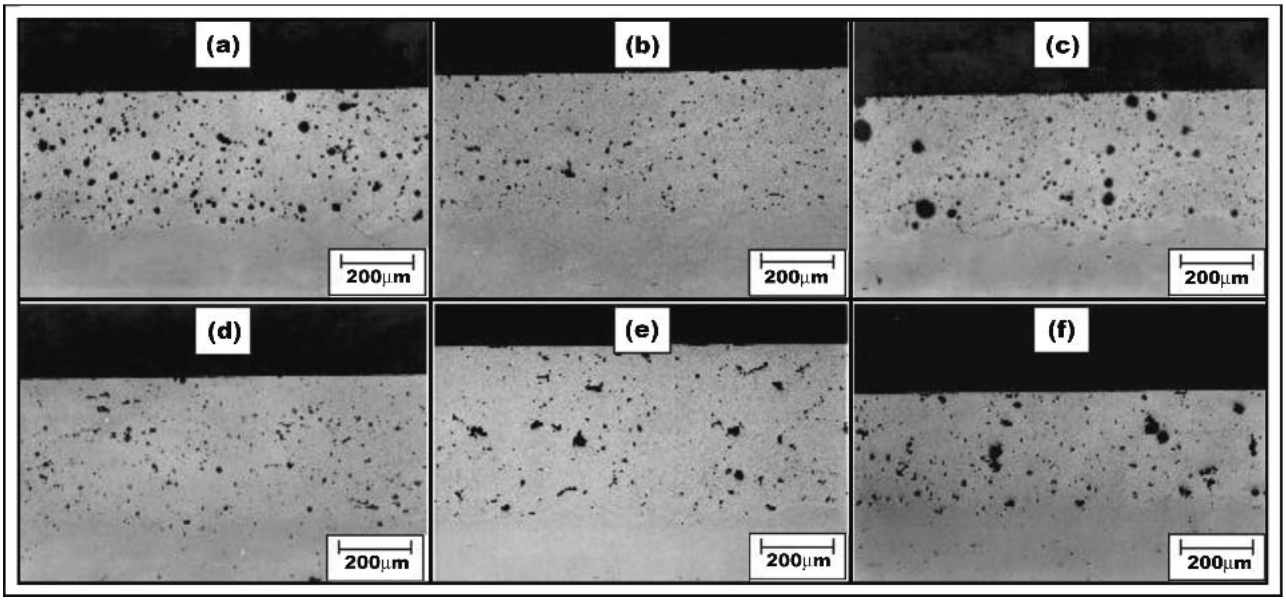

Fig. 3 Microstructures of the NiCrFeBSi coatings: **(a)** flame-fused Ø50 mm, **(b)** flame-fused Ø70 mm, **(c)** flame-fused Ø100 mm, **(d)** induction-fused Ø50 mm, **(e)** induction-fused Ø70 mm, and **(f)** induction-fused Ø100 mm

Table 4 Parameters Used for the Determination of Residual Strain by the $\sin^2 \psi$ XRD Method

Parameter	Value
Anode Type	Co
Anode Voltage, kV	40
Anode Current, mA	30
Peak Monitored	Ni ⟨220⟩, $2\theta = 91.770°$
Start Angle 2θ, °	86
Stop Angle 2θ, °	96
Step Size 2θ, °	0.05
Time per Step, s	15
χ Angle, °	−60°, −50°, . . . , 50°, 60°
Φ Angle, °	0°, 120°, 240°

of the sample at the three previously determined onset of cracking were evaluated (three values were obtained for the force and deflection respectively). For each sample, the force and deflection values obtained by these three procedures were averaged. The reported force (or stress) and deflection (or strain) needed for the onset of cracking are the averages of the values determined for each of the three samples tested for a specific fusing process and cylinder diameter. These reported values (stress or strain) gives a relative comparison of the ductility of each coating when exposed to a 4-point bending test. Therefore, this AE system combined with the bending test apparatus could be used to obtain important information on the relative ductility of thermal spray coatings.

2.4 Analysis and Characterization

Microhardness measurements of each coating were performed using a hardness tester (Model Durimet, Leitz GmbH, Wetzlar, Germany) equipped with a Vickers micro-indenter with a load of 300 gf. For each coating, a total number of five measurements were performed and the reported value is the average. Hardness measurements were also performed onto the underlying substrate material only, at different depths to see the influence of the fusing process onto the properties of the substrate. This hardness depth profile was performed onto a cross-section of the samples using a load of 5000 gf. For each depth position, a total number of five measurements were performed and an average value was reported.

Thermal spray coatings are well known to have residual strain. Therefore, to determine precisely the strain to fracture, the amount of residual strain present in the coatings has to be measured prior to perform the bend test. Stressed coatings exhibit a change of lattice spacing due to the internal strain present in the coating material. By using the obtained x-ray pattern of the coating, the measurements of peak positions results in the determination of the internal strain in the coatings. This calculated strain might be transformed to stress values using the modulus of elasticity of the coating. Therefore, strain and stress measurements were performed using an x-ray diffractometer (XRD) (Model 3000, Rich. Seifert & Co. GmbH & Co. KG, Ahrensburg, Germany) prior to the bending tests. These measurements resulted in the determination of the initial residual stress encountered in the thermal spray coatings. The parameters used for the residual strain and stress determination are presented in Table 4. For each combination cylinder diameter-fusing process, only two samples out of four were used for measuring the residual strain and stress.

The residual stress determination was performed using x-ray analysis software (RAYFLEX Analyze Software, Rich. Seifert & Co. GmbH & Co. KG) using the $\sin^2\psi$ XRD method.[12] For each diffraction pattern obtained, a peak fitting procedure was used to determine precisely the position of the peaks. From these determined peak positions, the strain and stress of the samples were calculated using known mechanical bulk properties of Ni.

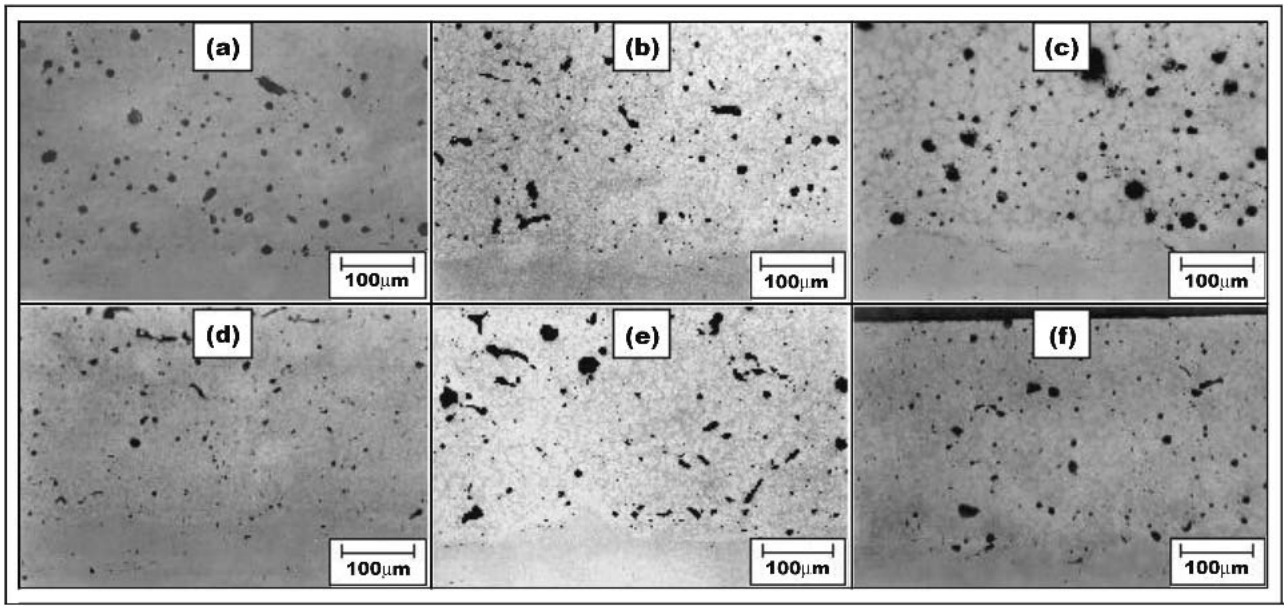

Fig. 4 Higher magnification of the coatings shown in Fig. 3: **(a)** flame-fused Ø50 mm, **(b)** flame-fused Ø70 mm, **(c)** flame-fused Ø100 mm, **(d)** induction-fused Ø50 mm, **(e)** induction-fused Ø70 mm, and **(f)** induction-fused Ø100 mm

Prior to performing the bending tests, the surface of the different samples were also analyzed using an optical microscope to compare the initial surface of the coatings to the cracked surface obtained after the bending test. This enables the possibility to obtain a qualitative observation of the degree of cracking of the coatings surface.

3. Results and Discussion

3.1 Coatings Microstructures

Micrographs shown in Figs. 3 and 4 reveal the microstructure of the coatings after being fused using either induction or flame method. An important feature is that no significant differences in microstructure can be observed between the coatings fused by induction or by flame process. Therefore, the use of either one of the fusing processes does result in similar coating microstructures. The porosity of the coatings looks quite different in Fig. 3 but a closer look on micrographs shown in Fig. 4, shows that the coatings seem to have a similar porosity value. However, as it will be shown later, the nature of the fusing process, either induction or flame, has some significant influences on other coating properties.

3.2 Hardness Measurements

Hardness results for each coating are presented in Fig. 5 for both induction and flame fusing process. A general trend can be observed from this figure, the coatings fused using the induction process always seem to have a slightly higher hardness than the coatings being fused using the flame process. However, taking the scattering of the values into consideration, one can say that there is no significant difference in hardness values of the thermal sprayed coatings under study, independently of the fusing process used. This result is in good correlation with the fact that the microstructures of the coatings are all quite similar for induction or flame-fused samples (see micrographs shown in Fig. 3 and 4).

Hardness results for each of the coated substrates are presented in Fig. 6 for both induction and flame-fused samples. No error bars are displayed for clarity purposes and the plotted line shows the general trend of the hardness values. The measurements were performed along the radius of a cross-section of the cylinders. Position 0 mm represents the interface between the coating and the substrate. The values presented in Fig. 6 should be compared with the hardness values measured for substrates before performing any fusing process: 292HV5.

The results show clearly that the hardness of the cylinders depends on the diameter and on the fusing process used. In general, for the cylinders fused using the induction process, the hardness is high at the surface of the substrate, within the first millimeters, with a value comparable to the raw substrate material, and then, the hardness stabilizes or decreases to lower values towards the center of the rod. For the cylinders fused using the flame process, the hardness is quite uniform throughout the substrate, with a value, which is relatively lower than for the raw substrate material, except for the smallest cylinder (diameter of 50 mm). For this small cylinder, the hardness is constant over the first 15 mm of the substrate with a value, which is higher than for the raw substrate material and then decreases towards the center of the rod. These hardness behaviors may be explained by the characteristics of the different fusing processes. The rods fused using the induction method are exposed to a shorter fusing and cooling time than the ones fused by the flame fusing process. Therefore, a higher quenching rate exists for the induction fusing method. This higher quenching rate results in less coarsening of the microstructure.

By comparing the results from the two different fusing pro-

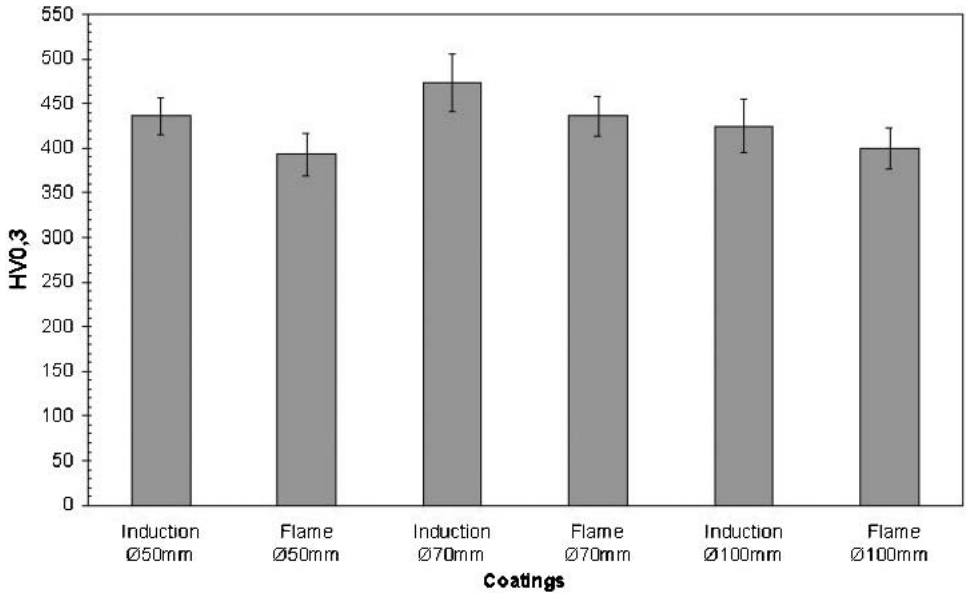

Fig. 5 Hardness of the thermal sprayed coatings after the fusing process

cesses, it can be observed that the hardness of the induction-fused substrate is higher than that of the flame-fused substrate, except for the smallest cylinder. These higher values for the induction-fused samples may be explained by the quenching effect due to the shorter heating and cooling time, as mentioned above. However, for the cylinder having the smaller diameter, this quenching effect has probably no important influence since the heat from the fusing process is probably diffused throughout the cylinder, due to its small diameter.

3.3 Residual Stress

The residual stress and strain results of the different sprayed and fused samples are presented in Fig. 7. As discussed previously, for each combination cylinder diameter-fusing process, only two out of four samples were used for the stress determination. The reported results are the average of these two distinct measurements and the error bars represent their range. The results show clearly that, independently of the cylinder diameter and fusing process, all the coatings under study were in a compressive state after being fused. A general tendency can be identified when analyzing the results shown in Fig. 7. Independently of the cylinder diameter, the flame fusing process produces coatings with a higher compressive stress state then the induction fusing process. This is mostly due to the different heat input characteristic of each fusing process. The residual stresses arising from fusing processes are mostly due to temperature difference between the coating and the cylinder core during the fusing process and also from their different cooling rates after the fusing process.

Figure 7 also shows that for a given fusing process (flame or induction), the residual stress decreases as the cylinder diameter is increased. However, this effect is more pronounced for the induction process than for the flame fusing process.

3.4 Typical Bend Testing Results

A typical curve of the force applied in function of the deflection of a sample during a bend test is shown in Fig. 8. This curve could be separated in 3 distinct regions as shown in Fig. 8: region I in which the sample is in an elastic state, where the force applied and the deflection have an linear relationship, region II where the sample is in a plastic state and deforms permanently under the application of the external force and region III, which represents the removal of the applied force (at the end of the test) and shows again the same elastic behavior as encountered in region I. The permanent deflection produced at the end of the bending test caused by the plastic deformation of the sample can be easily identified and measured from this type of curve, and for the example shown in Fig. 8, the permanent deflection is approximately equal to 7.8 mm.

Elastic properties, such as the modulus of elasticity of the samples could be derived from Fig. 8. The modulus of elasticity can be calculated using the slope of the curve force-deflection in the linear section (region I or III) using Eq 3 in Section 2.2.

Figure 8 shows also the cumulative number of AE signals (one of the three parameters selected for the determination of the onset of cracking) acquired during the bend test. From this example, the cracking of the coating was determined to begin at an applied force of approximately 7800 N and a deflection of 5.25 mm, which represents an applied stress of 770 MPa and a strain of 1.35%. However, as previously explained, the force and deflection (or stress and strain) needed for producing cracks in the coatings were also determined using two other selected parameters (amplitude and energy) and averaged. For comparison purposes, Table 5 lists the force and stress at cracking determined using the three different AE parameters for the bend test of the sample shown in Fig. 8. For all the samples and for all the tests performed, the difference between the force and stress values determined using the three different AE parameters is of the order of 5%.

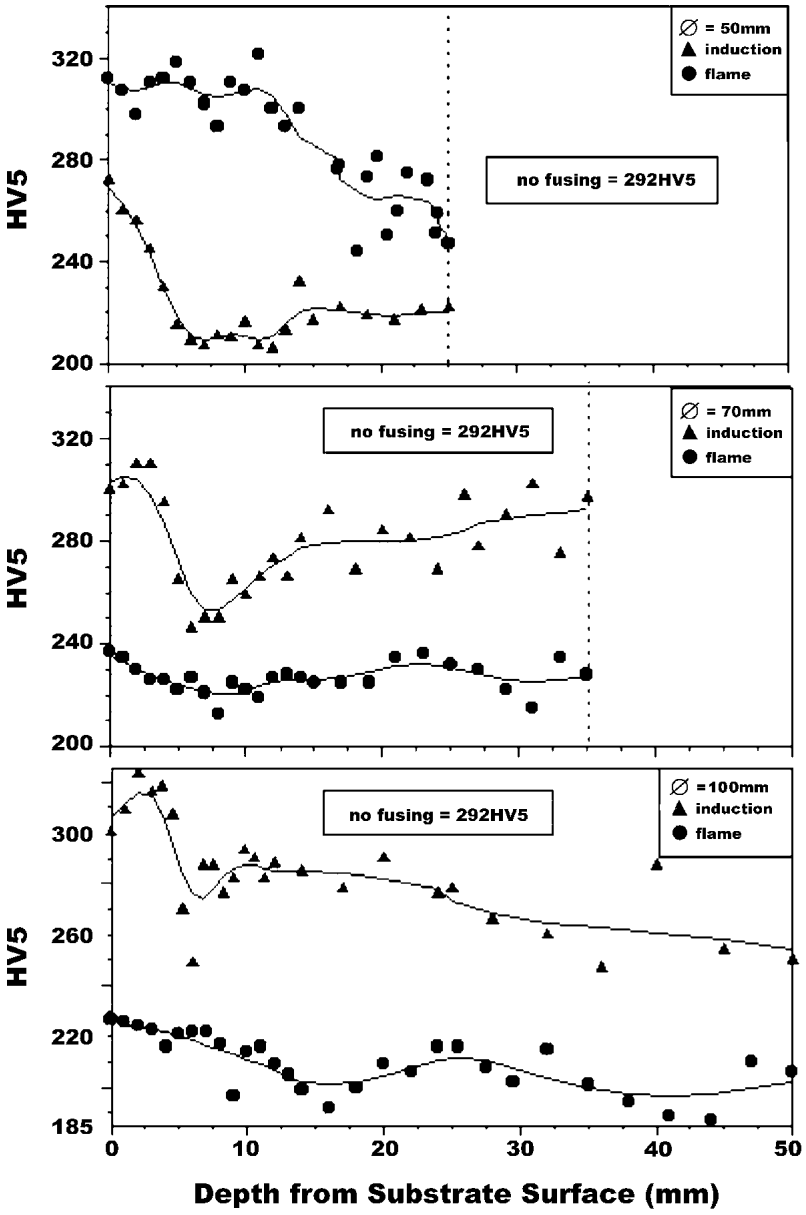

Fig. 6 Hardness of the 42CrMoS4 substrates after being thermal sprayed and fused

3.5 Determination of the Onset of Cracking

The strain necessary for the onset of cracking, also named the strain to fracture, for the different samples under study is shown in Fig. 9. This strain to fracture is equal to the applied strain to which the residual strain has been added (strain to fracture = applied strain + residual strain). For all cylinder diameters, the strain to fracture is higher for flame-fused samples than for induction-fused samples. Figure 9 also shows that there is a correlation between the residual strain and the strain to fracture. Samples having a high compressive residual strain exhibits a high strain to fracture. It is obvious from the results shown in Fig. 9 that for a specified fusing process, either flame or induction, that the strain to fracture does not change monotonically with the cylinder diameter value. Therefore, in addition to the cylinder diameter, other parameters, such as the modulus of elasticity and the yield strength of the samples which are both influenced by the different heat input rate of the fusing processes, also have an important effect onto the strain to fracture of the coatings. However, the exact magnitude of the influence of these parameters are not fully understood at this moment and further investigations are currently underway. Nevertheless, from these results, it is obvious that the sample with a 70 mm diameter fused by the flame process has the highest strain to fracture and therefore, this coating has the highest ductility of all the coatings tested for this study. The sample with a 100 mm diameter fused by induction process has the worst strain to fracture value and all the other coatings possess similar strain to fracture values.

Figure 10 shows the strain to fracture in comparison with the bending strain induced in the coating when rectifying a cylinder.

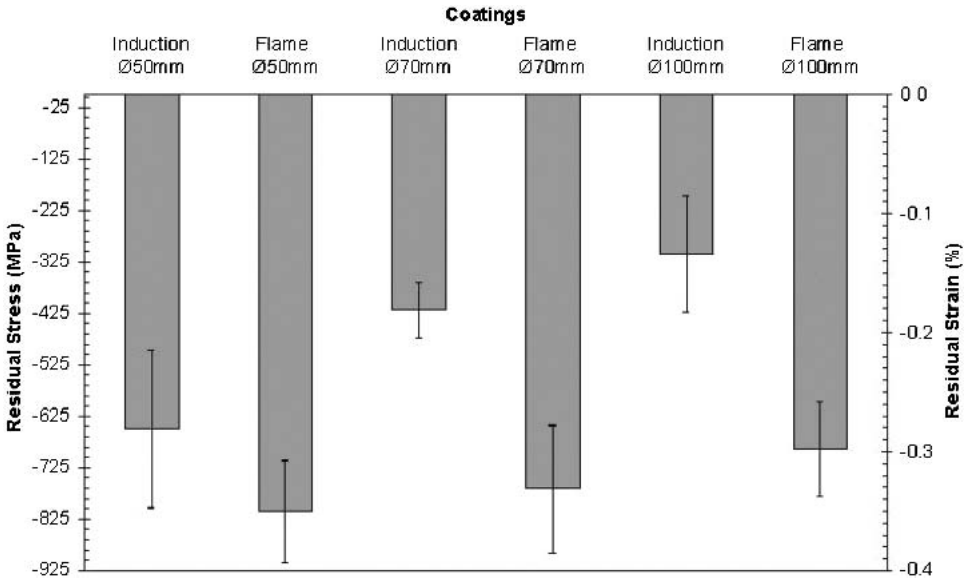

Fig. 7 Residual stress and strain present in the sprayed and fused samples determined by the $\sin^2\psi$ XRD method

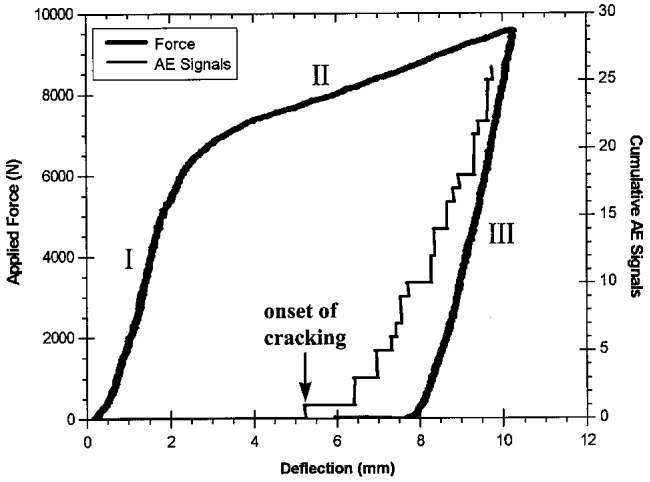

Fig. 8 Force applied and deflection of a sample during a typical 4-point bending test

The bending strain has been calculated for each cylinder diameter and for three different deflection values (5, 7, and 9 mm) at mid-span of a 1 m long cylinder. As can be observed, a minimal rectification involving a deflection of 5 mm does not represent any danger for the coatings except for the 100 mm induction fused cylinder, for which this rectification induces a strain in the coating which is almost equal to the strain to fracture of the coating. Therefore, for deflection values higher than 5 mm, the coating on the 100 mm induction fused cylinder would crack and would not be usable for any engineering application. All the other cylinders may experience higher deflection values before the strain induced by the rectification could be of the same magnitude of the strain to fracture. However, it can be seen that for the 100 mm flame-fused cylinder, a deflection of 9 mm induces a strain, which is almost equal to the strain to fracture of the coating. For this sample, a rectification with a deflection higher than 7 mm may be problematic by inducing cracks in the coating. Again, from the results shown in Fig. 10, it is obvious that the sample with a 70 mm diameter fused by flame process is the coating having the highest ductility. This coating may undergo severe rectification by bending before experiencing any failure due to cracking.

The surface of the different samples before and after being tested in the 4-point bending test can be seen in Fig. 11 and 12, respectively. From Fig. 11, it is observed that all the samples have a polished surface without the presence of any cracks. Figure 12 shows the surface of the samples after the bend test and shows different degree of cracking. Cracks are clearly visible and are identified on each micrographs of Fig. 12. However, it should be noted that the photos of the surfaces after the bend test are not taken at the same applied stress for all samples. Therefore, the more ductile sample, the one having the higher crack resistance, is not necessarily the one with a surface having the least number of cracks after the bend test, since the stress value at the end of the test for this ductile sample could be at a higher relative value compared with the stress needed for cracking than the worst ductile coating. For a more comprehensive understanding of the photos shown in Fig. 12 and of the previously mentioned statement, Table 6 lists the values of the maximum applied strain at the end of the bend test, the strain to fracture and their ratio. The ratio represents a qualitative measure of the severity of the damages (cracks) undergone by the samples when submitted to the 4-point bend test system when the final load is different for all the tests.

A high ratio means that the final load (strain) applied on the sample is significantly higher that the load (strain) to fracture of the coating. Therefore, a high ratio means a high number of cracks in the coatings at the end of the bend tests. As shown in Table 6, the ranking of the different samples places the flame 50 mm sample as the one having the lowest ratio and the flame 100 mm as the sample having the highest ratio. The same rank-

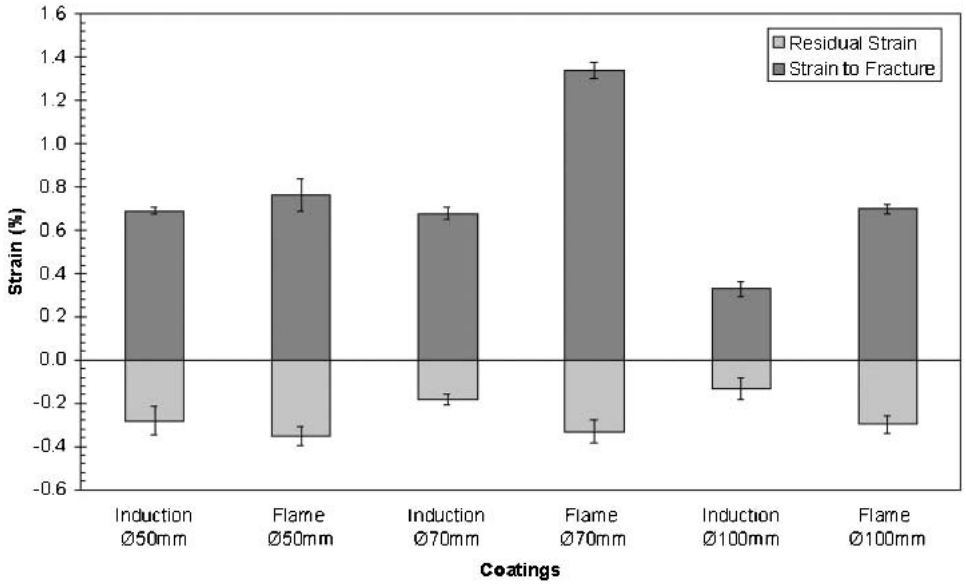

Fig. 9 Strain to fracture values and residual strain for the NiCrFeBSi self-fluxing coatings

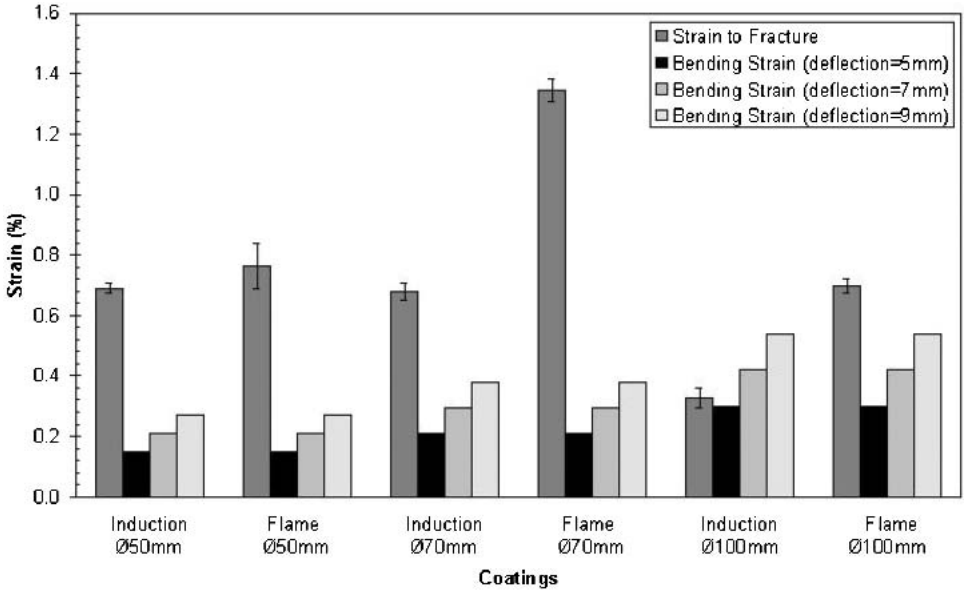

Fig. 10 Strain to fracture values and bending induced strain during rectification of a 1 m long cylinder sprayed with NiCrFeBSi self-fluxing coatings

Table 5 Comparison of the Force and Stress at Cracking Determined by the Three Different AE Parameters for the Sample Shown in Fig. 8

AE Parameter	Force at Cracking, N	Stress at Cracking, MPa	Average Force, N	Average Stress, MPa	(Max-Min)/Average (for Force and Stress) %
Number of AE	7800	766			
Amplitude of AE	7400	727	7567	743	5.4
Energy of AE	7500	736			

ing as the one listed in Table 6 could be relatively observed on the micrographs of Fig. 12, with the flame 50 mm sample having a few very small cracks and the flame 100 mm sample having an important number of large cracks. Therefore, the photos shown in Fig. 12 are quite correlated with the ratio given in Table 6.

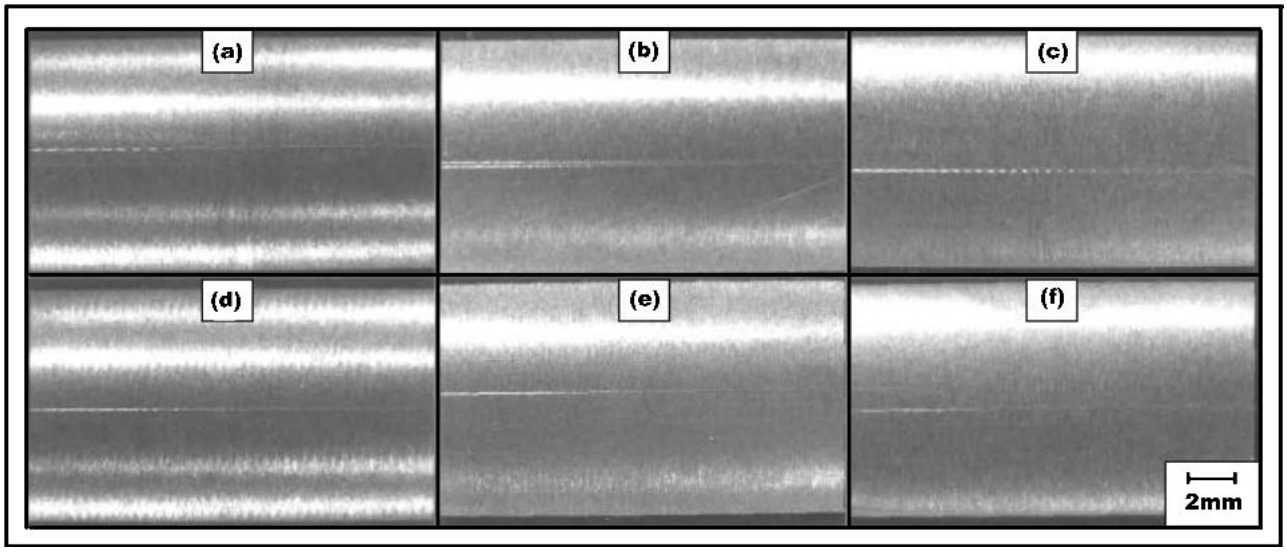

Fig. 11 Micrographs showing the surface of the samples before performing the bend test: **(a)** flame-fused Ø50 mm, **(b)** flame-fused Ø70 mm, **(c)** flame-fused Ø100 mm, **(d)** induction-fused Ø50 mm, **(e)** induction-fused Ø70 mm, and **(f)** induction-fused Ø100 mm

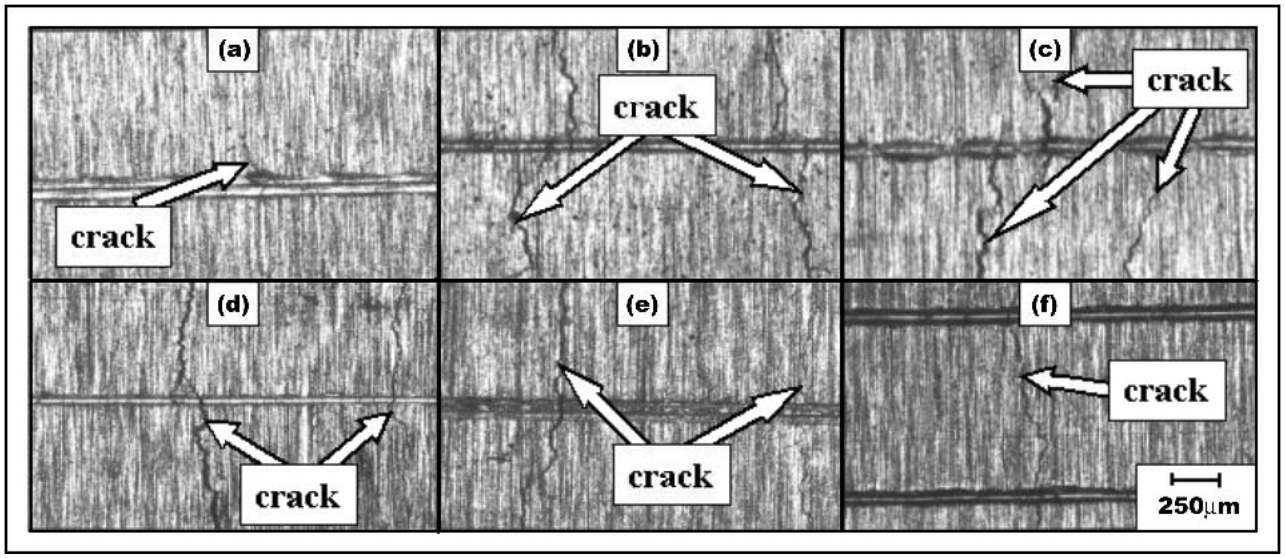

Fig. 12 Micrographs showing the surface of the samples after performing the bend test: **(a)** flame-fused Ø50 mm, **(b)** flame-fused Ø70 mm, **(c)** flame-fused Ø100 mm, **(d)** induction-fused Ø50 mm, **(e)** induction-fused Ø70 mm, and **(f)** induction-fused Ø100 mm

Table 6 Comparison of the Maximum Applied Strain and the Strain to Fracture for the Different Samples Under Study

Sample	Maximum Applied Strain, %	Strain to Fracture, %	Ratio Applied/Fracture Strain	Ratio Rank (1 = lowest, 6 = highest)
Induction 50 mm	1.979	0.690	2.87	5
Induction 70 mm	1.339	0.677	1.98	3
Induction 100 mm	0.656	0.328	2.00	4
Flame 50 mm	0.929	0.762	1.22	1
Flame 70 mm	2.238	1.343	1.67	2
Flame 100 mm	2.292	0.699	3.28	6

4. Conclusions

The type of fusing process, either induction or flame fusing, used on thermal sprayed NiCrFeBSi self-fluxing alloys and the diameter of the cylindrical substrate both seem to have only a minor effect on the microstructure and hardness of the coatings. However, the hardness of the underlying steel substrate is greatly influenced by both the fusing process and the diameter of the substrate.

For the induction-fused samples, a quenching effect due to the shorter fusing and cooling time associated with this process may be present. This quenching effect results in a higher hardness at the surface of the cylinder than in its core. On the other hand, the more constant hardness values throughout the cylinders fused with the flame process may be attributed to the lack of one such quenching effect due to the longer fusing and cooling time associated with it.

All the coatings under study are in a compressive stress state. Independently of the cylinder substrate diameter, the flame-fused samples all have a greater stress magnitude than their induction-fused counterparts.

It was observed that the flame-fused coatings all possess a higher strain to fracture than their induction-fused counterparts. Therefore, for a fixed cylindrical substrate diameter, the flame-fused coatings have a higher ductility and may experience higher bending strains before cracking could occur in their microstructure. From all the coatings tested in this study, the flame-fused coating sprayed on a 70 mm diameter cylinder possessed the highest strain to fracture (1.34%). On the other hand, the induction-fused coating sprayed on a 100 mm diameter cylinder possessed the lowest strain to fracture (0.328%). All the four other coatings possessed similar strain to fracture values, ranging from 0.68% to 0.76%. For comparison purposes, the strain to fracture of the best coating represents a mid-span deflection of 31.9 mm for a 1 m long cylinder having a 70 mm diameter and is equal to 5.5 mm for the worst coating sprayed on a 1 m long cylinder having a diameter of 100 mm. Therefore, the latter coating could easily crack under light bending rectification.

Finally, this work points out that the combination of an AE technique with a bending test apparatus shows some major benefits to obtain important information on the relative strain to fracture or ductility of thermal spray coatings.

Acknowledgments

We gratefully acknowledge Assmann Metallspritztechnik GmbH (Rhede, Germany) for thermal spraying and fusing the samples and Linde Gas AG (Höllriegelskreuth, Germany) for cutting the sprayed and fused cylinders into samples adequate for the bend testing apparatus.

References

1. D. Dalmas, S. Benmedakhene, C. Richard, A. Laksimi, T. Gregoire: "Characterization of Cracking Within WC-Co Coated Materials by an Acoustic Emission Method During Four Points Bending Tests" in *Thermal Spray: Surface Engineering via Applied Research*, C.C. Berndt, ed., ASM International, Materials Park, OH, 2000, pp. 1335-40.
2. L.C. Cox: "The Four-Point Bend Test as a Tool for Coating Characterization" in *Proceedings of the 15th International Conference on Metallurgical Coatings*, R.C. Krutenat, ed., Elsevier Applied Science, London, UK, 1988, pp. 807-15.
3. U. Wiklund, M. Bromark, M. Larsson, P. Hedenqvist, and S. Hogmark: "Cracking Resistance of Thin Hard Coatings Estimated by Four-Point Bending," *Surf. Coating Technol.*, 1997, *91,* pp. 57-63.
4. U. Wiklund, P. Hedenqvist, S. Hogmark: "Multilayer Cracking Resistance in Bending," *Surf. Coating Technol.*, 1997, *97,* pp. 773-778.
5. S. Hogmark, S. Jacobson, and M. Larsson: "Design and Evaluation of Tribological Coatings," *Wear*, 2000, *246,* pp. 20-33.
6. R. Westergård, N. Axén, U. Wiklund, and S. Hogmark: "An Evaluation of Plasma Sprayed Ceramic Coatings by Erosion, Abrasion, and Bend Testing," *Wear*, 2000, pp. 12-19.
7. L. Manes, J-M. Monicault, R. Gras: "Monitoring Damage by Acoustic Emission in Bearing Steels in Cryogenic Environment," *Tribol. Int.*, 2001, *34,* pp. 247-253.
8. J. Miettinen, P. Andersson: "Acoustic Emission of Rolling Bearings Lubricated With Contaminated Grease," *Tribol. Int.*, 2000, 33, pp. 777-87.
9. C.K. Lin, C.C. Berndt, S. Leigh, and K. Murakami: "Acoustic Emissions Studies of Alumina-13% Titania Freestanding Forms During Four Point Bend Tests," *J. Am. Ceram. Soc.*, 1997, *80*(9), pp. 2382-94.
10. J. Voyer: "Etude d′Èmission Acoustique de Barrières Thermiques Sous des Conditions de Chargement Thermique Cyclique," Ph.D. Thesis, Université de Sherbrooke, Sherbrooke, Canada, 1997, ISBN 0612264041 (in French).
11. Anon: *Metals Handbook—Mechanical Testing*, Vol. 8, 9th ed., ASM International, Materials Park, OH, 1985, pp. 1–778.
12. I.C. Noyan and J.B. Cohen: *Residual Stresses Measurement by Diffraction and Interpretation*, Springer-Verlag, New York, NY, 1987, pp. 1-276.